

## Retraction

# Retracted: Macro-Micro Study on Mechanical Properties of Frozen Fine Sandstone Based on DEM Mathematical Model

### Journal of Function Spaces

Received 12 December 2023; Accepted 12 December 2023; Published 13 December 2023

Copyright © 2023 Journal of Function Spaces. This is an open access article distributed under the Creative Commons Attribution License, which permits unrestricted use, distribution, and reproduction in any medium, provided the original work is properly cited.

This article has been retracted by Hindawi, as publisher, following an investigation undertaken by the publisher [1]. This investigation has uncovered evidence of systematic manipulation of the publication and peer-review process. We cannot, therefore, vouch for the reliability or integrity of this article.

Please note that this notice is intended solely to alert readers that the peer-review process of this article has been compromised.

Wiley and Hindawi regret that the usual quality checks did not identify these issues before publication and have since put additional measures in place to safeguard research integrity.

We wish to credit our Research Integrity and Research Publishing teams and anonymous and named external researchers and research integrity experts for contributing to this investigation.

The corresponding author, as the representative of all authors, has been given the opportunity to register their agreement or disagreement to this retraction. We have kept a record of any response received.

## References

- [1] M. Ma, M. You, S. Peng, B. Zhang, and Y. Lin, "Macro-Micro Study on Mechanical Properties of Frozen Fine Sandstone Based on DEM Mathematical Model," *Journal of Function Spaces*, vol. 2022, Article ID 7176665, 10 pages, 2022.

## Research Article

# Macro-Micro Study on Mechanical Properties of Frozen Fine Sandstone Based on DEM Mathematical Model

Maoyan Ma<sup>1</sup>, Min You<sup>1</sup>, Shuguang Peng<sup>1</sup>, Biao Zhang<sup>2</sup>, and Yuan Lin<sup>3</sup>

<sup>1</sup>Anhui Province Key Laboratory of Building Structure and Underground Engineering, Anhui Jianzhu University, Hefei 230601, China

<sup>2</sup>Jining Planning and Design Institute, Jining 272100, China

<sup>3</sup>School of Environment and Energy Engineering, Anhui Jianzhu University, Hefei 230601, China

Correspondence should be addressed to Maoyan Ma; [maoyanma2019@163.com](mailto:maoyanma2019@163.com).

Received 4 April 2022; Accepted 27 April 2022; Published 16 May 2022

Academic Editor: Miaocho Chen

Copyright © 2022 Maoyan Ma et al. This is an open access article distributed under the Creative Commons Attribution License, which permits unrestricted use, distribution, and reproduction in any medium, provided the original work is properly cited.

The study of freezing rock mechanical properties is getting more and more urgent because of coal mine construction in western China. Particle discrete element method (DEM) can describe discontinuous medium problem mathematically. In order to reveal the mechanical failure mechanism of frozen fine sandstone, the uniaxial compressive strength test of frozen fine sandstone was carried out, and then, DEM was used to simulate the uniaxial test of frozen fine sandstone. Furthermore, the nuclear magnetic resonance (NMR) technology was used to obtain pore distribution of the freezing sandstone. Finally, the results of NMR test and discrete element simulation were combined to reveal the microscopic mechanism of mechanical change in freezing fine sandstone. The DEM results show that the strength of frozen fine sandstone increases with the decrease of temperature. With the decrease of temperatures, strain softening occurs in frozen sandstone, which indicates that the discrete element simulation results are in good agreement with the uniaxial test results. Therefore, DEM can be used to simulate the mechanical behavior of frozen fine sandstone. At the same time, the DEM results also indicate that the formation and development of the shear band are the precursor of the failure of the sample. Furthermore, the NMR test confirms that temperature has a great impact on the pore distribution of sandstone. With the decrease of temperature, the pore ice content increases greatly, which induces a great decrease in NMR porosity and a vast decrease in the proportion of large and medium pores in all pores. Meanwhile, with the growth of the cohesion induced by increasing ice content, the uniaxial compressive strength increases macroscopically.

## 1. Introduction

With the development of coal mining in western China, the number of mine shafts constructed by freezing method in these areas is increasing. Shafts need to pass through deep bedrocks such as Cretaceous and Jurassic strata, which are characterized by poor rock cementation and easy to be softened in water. Different from the freezing sinking in deep alluvium in the eastern region, the previous design parameters and construction experience cannot scientifically guide the mine construction in the western region [1–5]. Furthermore, the research on the mechanical behavior of laboratory frozen rock needs to be equipped with a temperature control system, and the technical requirements are higher than those of conventional geotechnical tests. Therefore, numerical

simulation is often used as an effective and necessary supplement to the frozen rock test technology. Frozen rock is a discrete particle aggregation composed of multiphase media, and particle discrete element method (DEM) is a method for studying the characteristics of granular materials [6, 7]. Therefore, DEM can be used to simulate the mechanical properties of laboratory frozen rock [8–13].

At present, many researchers have made a series of achievements in the study of mechanical behavior of laboratory rock and soil by using discrete element method. Belheine et al. [14] simulated triaxial tests of sand under drainage conditions by using three-dimensional spherical discrete element model with rolling stiffness. Kozicki et al. [15] studied the influence of initial porosity and particle shape by simulating triaxial tests of sand under drainage

conditions using three-dimensional DEM. De Bono et al. [16] conducted discrete element simulation on the triaxial test of crushed cemented sand. Hu et al. [17] established a damage and fracture model of rock aging deformation based on discrete element method and used this model to conduct numerical simulation research on the creep instability and failure process of rock under different stress levels. Zhou et al. [18] used the two-dimensional discrete element method to numerically simulate the laboratory plane strain test of frozen sand and used the model of bond occurring within a small range of contact points to consider the role of ice in frozen soil. Yin et al. [19] used the parallel bond model to simulate the triaxial test of frozen clay under different temperatures and confining pressures. Yuan et al. [20] used the parallel bond model to describe the interaction between soil particles and between ice and soil particles. Using nuclear magnetic resonance technology (NMR), the pore structure characteristics of rock and soil can be visually displayed, which provides a powerful means for the study of micro mechanism of rock and soil [21, 22].

However, the application of discrete element in frozen rock research still needs to solve many problems, especially the selection of model which is extremely important. In this paper, DEM was used to simulate the laboratory uniaxial test of frozen fine sandstone. The model that the bond occurs in the finite range between the contact particles was used to consider the bonding effect of ice in frozen sandstone. This model can simulate the bonding process of particles after loading and is suitable for describing the constitutive characteristics of interlayer materials in the finite range between particles. In view of the limitations of numerical simulation, NMR was used to obtain the pore distribution inside the rock during freezing. Combined with the results of DEM numerical simulation, the microscopic mechanism of the frozen fine sandstone was revealed.

## 2. Material and Methods

**2.1. Samples.** The rock samples were taken from the Jurassic strata in western China and processed into standard samples of  $\Phi 50 \text{ mm} \times 100 \text{ mm}$  (see Figure 1) for uniaxial compression tests. Samples were screened by HC-F800 acoustic wave tester to ensure that the test rock samples have no original cracks. At the same time, the sandstone was processed into  $\Phi 25 \text{ mm} \times 60 \text{ mm}$  for NMR tests after being saturated.

### 2.2. Methods

**2.2.1. Uniaxial Compression Strength Test.** The test was carried out according to standard test procedure for physical and mechanical properties of artificial freezing rock and soil (MT/T593-1996) and geotechnical engineering test method and criterion (GB/T50123-2009). The sample was immersed in a closed water cylinder for pumping treatment, followed by continuous immersion for 24 h. The saturated rock samples were put into the low-temperature tank with preset temperature, and the freezing rate was set to  $1^\circ\text{C}/\text{h}$ . After freezing for 48 h, the samples were put on rubber sleeves and placed on the MTS compression test machine for uniax-



FIGURE 1: The standard sample.

ial compressive strength test. DX-40 low-temperature numerical control test chamber was used in the test. The temperature control range was  $-40$  to  $0$  degrees Celsius with the temperature control accuracy of  $\pm 2^\circ\text{C}$ , and the temperature was automatically controlled. In order to meet the actual needs of freezing shaft construction in western China, uniaxial compression test was carried out at  $20^\circ\text{C}$ ,  $-2^\circ\text{C}$ ,  $-5^\circ\text{C}$ ,  $-8^\circ\text{C}$ ,  $-11^\circ\text{C}$ , and  $-15^\circ\text{C}$ .

**2.2.2. NMR Test.** MesoMR23-060H-I low-temperature nuclear magnetic resonance micro structure analysis and imaging system was used (Figure 2) in this test. The processed fine sandstone samples were maintained at  $1 \text{ MPa}$  in the vacuum pressure saturation equipment for 24 h. The samples were taken out and put into the nuclear magnetic resonance equipment to measure the porosity of the rock sample at five temperature levels of  $20^\circ\text{C}$ ,  $-2^\circ\text{C}$ ,  $-5^\circ\text{C}$ ,  $-8^\circ\text{C}$ ,  $-11^\circ\text{C}$ , and  $-15^\circ\text{C}$ .

## 3. Basic Theory of DEM

The discrete element model can discrete the simulation object into discontinuous particles and define the transmission of force or force moment between particles, which can reflect the discontinuity and anisotropy of rock materials. PFC is a discrete element software using particle aggregates to characterize materials. Based on Newton's second law and the relationship between force and displacement, it can simulate the movement of circular particles and their interaction and can also simulate the block structure problem by connecting two or more particles with their directly adjacent particles to form arbitrary shape combinations. The particle contact model in this paper adopts the parallel bond contact model. The parallel bond model can be used



FIGURE 2: The equipment for NMR test.

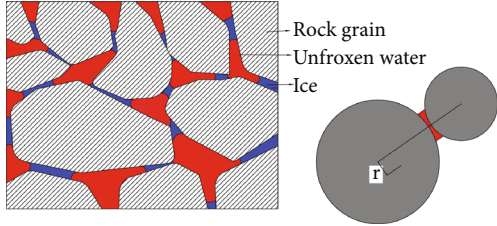


FIGURE 3: Diagram of frozen sandstone structure and parallel bond model.

to characterize the particle materials with large bonding force between particles, and the frozen rock has strong cohesive force due to the action of ice. The bonding structure diagram is shown in Figure 3. The contact model can transfer force and force moment between particles, limit relative sliding and rotation between particles, and give normal stiffness and tangential stiffness between particles. It can generate bond in a certain range of particle contact point to simulate the cementation between particles and provide normal tensile strength and shear strength of particles. The macroscopic mechanical behavior of frozen soil can be reproduced by adjusting the stiffness parameter, bond strength parameter and friction coefficient in the model.

In the parallel bond model, the bond stress follows the relationship between force and displacement. The force-displacement relationship of parallel bond is obtained by the normal and tangential stiffness, tensile and shear strength, bond radius factor, and other parameters. The force and force moment acting on the parallel bond can be expressed as  $F_i$  and  $M_i$  composing of components in normal and tangential directions and can be expressed as

$$\overline{F}_i = \overline{F}_i^n + \overline{F}_i^s, \quad (1)$$

$$\overline{M}_i = \overline{M}_i^n + \overline{M}_i^s, \quad (2)$$

where  $\overline{F}_i^n$  and  $\overline{M}_i^n$  are normal force and moment vectors, respectively, and  $\overline{F}_i^s$  and  $\overline{M}_i^s$  are tangential force and moment vectors, respectively.

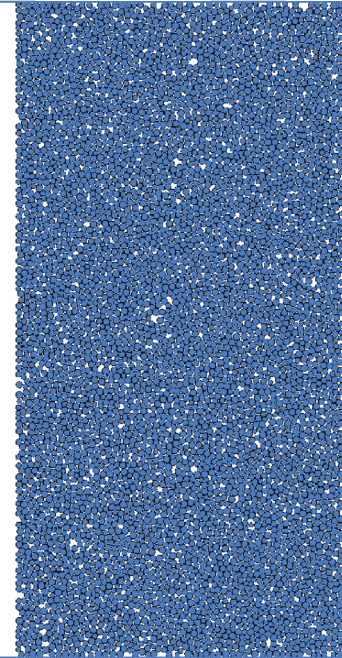


FIGURE 4: The generated sample.

Once the parallel bond is formed,  $F_i$  and  $M_i$  will be initialized to zero. The forces and force moments resulting from subsequent relative displacement increments and relative rotation increments will be superimposed on the current values. The force and moment generated by relative displacement increments and relative rotation increments can be expressed as

$$\begin{cases} \Delta\overline{F}_i^n = -k^n A \Delta u_i^n, \\ \Delta\overline{F}_i^s = -k^s A \Delta u_i^s, \\ \Delta\overline{M}_i = -k^n I \Delta \theta_i. \end{cases} \quad (3)$$

Among them,  $\Delta u_i = v_i \Delta t$ ,  $\Delta \theta_i = w_i \Delta t$ ,  $A = 2\bar{R}$ , and  $I = (2/3)\bar{R}^3$ , where  $\Delta\overline{F}_i^n$  and  $\Delta\overline{F}_i^s$  are the increment of normal and tangential bonding force respectively;  $\Delta\overline{M}_i$  is force

TABLE 1: Parameters of sandstone particle flow model.

| Temperature (°C) | Contact stiffness<br>( $\times 10^6$ kPa) |         | Bond strength<br>( $\times 10^6$ kPa) |        | Coefficient of friction | Pb_emod |
|------------------|---|---------|---------------------------------------|--------|-------------------------|---------|
|                  | Normal                                    | Tangent | Pb_coh                                | Pb_ten |                         |         |
| 20               | 10e8                                      | 10e8    | 35e6                                  | 25e6   | 0.50                    | 15e8    |
| -2               | 11e8                                      | 11e8    | 42e6                                  | 31e6   | 0.43                    | 18e8    |
| -5               | 12e8                                      | 12e8    | 45e6                                  | 33e6   | 0.41                    | 20e8    |
| -8               | 14e8                                      | 14e8    | 47e6                                  | 35e6   | 0.39                    | 24e8    |
| -11              | 16e8                                      | 16e8    | 50e6                                  | 37e6   | 0.35                    | 26e8    |
| -15              | 17e8                                      | 17e8    | 52e6                                  | 39e6   | 0.31                    | 27e8    |

moment increment;  $k^n$  and  $k^s$  are normal and tangential stiffness, respectively;  $A$  is bonding area;  $\Delta u_i^n$  and  $\Delta u_i^s$  are displacement increments in normal and tangential directions, respectively;  $\Delta\theta_i$  is relative rotation angle of contact particles;  $I$  is the inertia moment of the bonding surface on the neutral axis;  $v_i$  is the relative velocity of contact particles;  $w_i$  is relative angular velocity of contact particles;  $\bar{R}$  is contact bond radius; and  $\Delta t$  is time steps. The maximum tensile stress and shear stress acting on the parallel bond are

$$\bar{\sigma}_i^{\max} = \frac{\bar{F}_i^n}{A} + \frac{|\bar{M}_i^n| \bar{R}}{I}, \quad (4)$$

$$\bar{\tau}_i^{\max} = \frac{|\bar{F}_i^s|}{A}. \quad (5)$$

When the maximum tensile stress acting on the bond is larger than the ultimate tensile strength of the bond itself, the bond breaks and produces tensile cracks. Similarly, when the maximum shear stress acting on the bond exceeds the ultimate shear strength of the bond itself, the bond breaks and produces shear cracks.

#### 4. Discrete Element Simulation of Frozen Sandstone

**4.1. Simulation Process.** Firstly, the wall with the same size as the laboratory test sample was defined to load the sample. The model size was 100 mm in height and 50 mm in diameter, and the particles were filled inside the wall. Then, the suspended particles outside the model were eliminated, and the particles were adjusted to achieve uniform model (Figure 4). The contact type between particles was set as parallel bonding, and the model parameters were assigned. Finally, the model was axially loaded by the relative movement of the upper and lower walls, and axial strain and axial stress were recorded.

In the process of simulation, in order to match the characteristics of laboratory sand test curve, a series of numerical simulation tests are needed. Before the numerical test results are basically consistent with the actual physical model test results, the input parameters of PFC model are adjusted repeatedly [23, 24].

For the parallel bond model used in this simulation, the mesoparameters such as the contact stiffness, bond strength, and friction coefficient of the model are adjusted to ensure

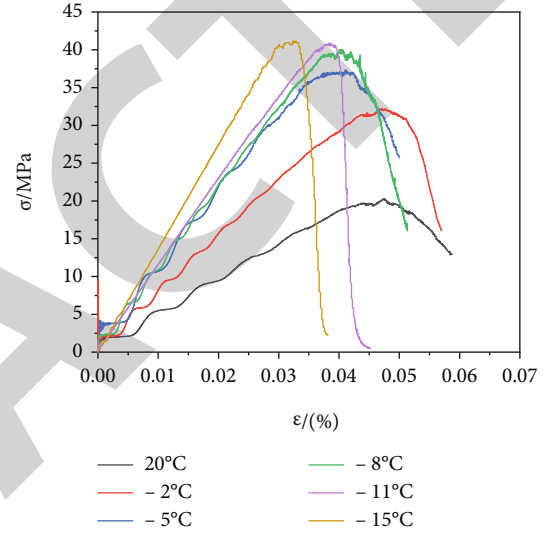


FIGURE 5: DEM calculating results under different soil temperature.

that the simulated stress-strain curves can conform to the stress-strain curves in the experiment. Due to the dependence of rock on temperature, the model parameters obtained at different freezing temperatures are different. Table 1 shows the basic parameters of the model.

**4.2. Discrete Element Analysis of Stress-Strain Relationship.** Discrete element simulation of frozen rock uniaxial compressive test was carried out at 20°C, -2°C, -5°C, -8°C, -11°C, and -15°C. The results have been shown in Figure 5. It can be seen from Figure 5 that the peak strength of frozen sandstone increases with the decrease of temperature. It increases from 20.3 MPa at 20°C to 41.6 MPa at -15°C. Table 1 shows that the microscopic parameters including the contact stiffness between particles and the bond strength between particles also increase accordingly; that is, the microscopic parameters have a strong temperature dependence, which is significantly different from the sandstone at normal temperature. With the decrease of temperature, water will gradually transform into ice, and the cementation of ice improves the cohesion of the sandstone. At the same time, the micro pores decrease accordingly, so that the strength of frozen sandstone is greatly improved, and with the decrease of temperatures, the failure type of the

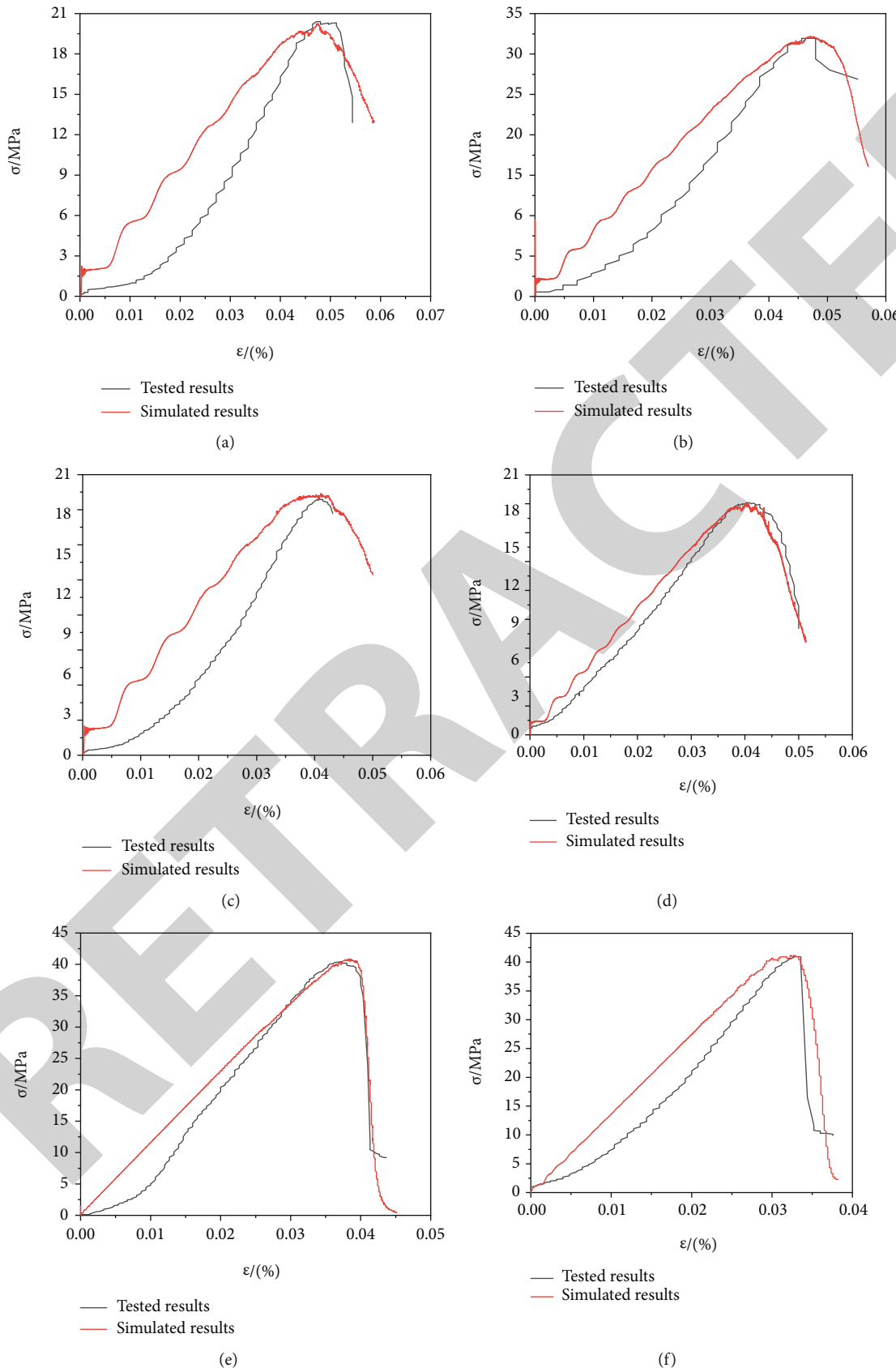


FIGURE 6: Comparison of discrete element numerical test and laboratory test: (a)  $20^{\circ}\text{C}$ ; (b)  $-2^{\circ}\text{C}$ ; (c)  $-5^{\circ}\text{C}$ ; (d)  $-8^{\circ}\text{C}$ ; (e)  $-11^{\circ}\text{C}$ ; (f)  $-15^{\circ}\text{C}$ .

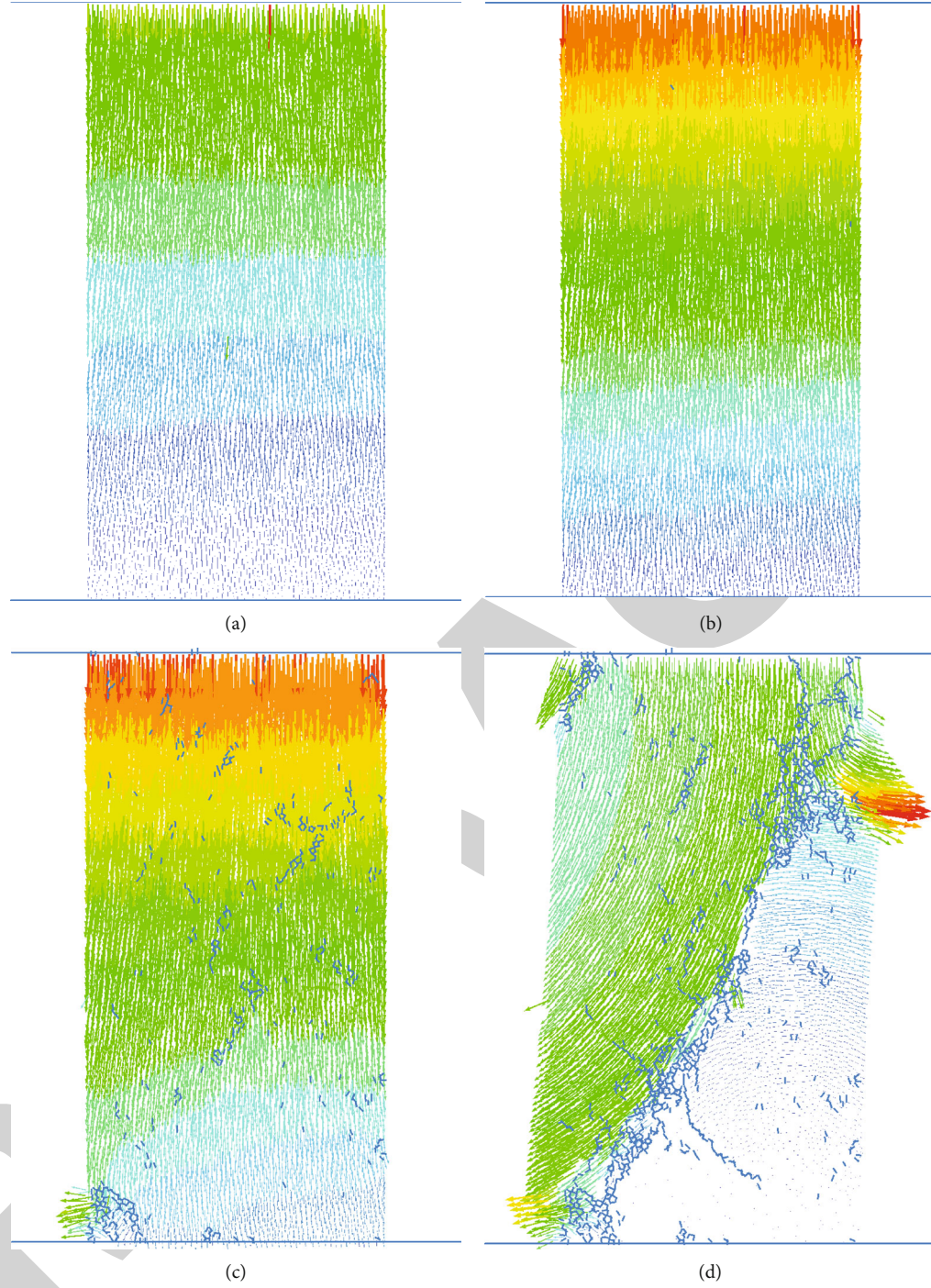


FIGURE 7: Displacement field distribution under different strains: (a)  $\varepsilon = 1\%$ ; (b)  $\varepsilon = 2.3\%$ ; (c)  $\varepsilon = 4.8\%$ ; (d)  $\varepsilon = 5.6\%$ .

sandstone changes from plasticity at high temperatures to brittleness at lower temperatures. In addition, as shown in Figure 5, with the decrease of temperature, the strain corresponding to the peak strength decreases from 4.8% at  $-5^{\circ}\text{C}$  to 3.2% at  $-15^{\circ}\text{C}$ . It shows that with the decrease of temperature, strain softening occurs in frozen sandstone.

Figure 6 shows that the simulation results are consistent with the laboratory uniaxial test results, which indicates that the discrete element method can be used to simulate the mechanical behavior of frozen sandstone.

**4.3. DEM Simulation of Shear Band Formation and Development.** At the temperature of  $-5^{\circ}\text{C}$ , the displacement field under different strains is obtained by DEM, which has been shown as Figure 7. The criterion for judging the beginning of shear band formation is that the stress-strain curve is at the peak point [25]. In this study, the strain corresponding to the peak of the stress-strain curve is 4.8%; therefore, 4.8% is taken as the failure strain. The formation and development of the displacement are corresponding to the change trend of the stress-strain curve. The curve at the temperature

TABLE 2: NMR porosity of saturated fine sandstone at different temperatures.

| Temperature (°C) | 20  | -2  | -5  | -8  | -11 | -15 |
|------------------|-----|-----|-----|-----|-----|-----|
| NMR porosity (%) | 9.1 | 3.8 | 1.5 | 1.2 | 1.1 | 1.1 |

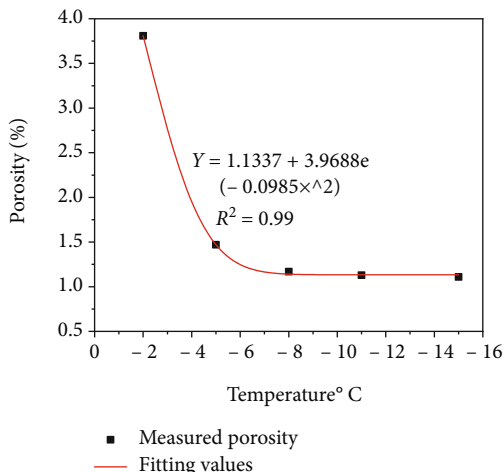


FIGURE 8: Relationship between NMR porosity and temperature.

of  $-5^{\circ}\text{C}$  in Figure 5 corresponds to the change process of displacement field in Figure 7. The displacement field of strain 1% and 2.3% in Figure 7 corresponds to the rising curve of  $-5^{\circ}\text{C}$  in Figure 5. When the displacement field begins to appear, obvious uneven distribution, damage, or micro cracks begin to appear (see Figure 7(b)). When the strain is 4.8%, corresponding to the peak of the curve, the micro cracks continue to increase, and the shear band begins to form (see Figure 7(c)). The strain value of 5.6% corresponds to the curve after the peak. With the increase of strain, the micro cracks gradually increase and develop into shear bands (see Figure 7(d)). At the same time, the uniform distribution of particle displacement is obvious, and the volume of the sample increases continuously. Finally, a stable shear band from left to right is formed. The corresponding macroscopic deformation occurs after reaching the peak. The displacement field distribution at other temperatures also has a similar corresponding relationship with the macroscopic stress-strain curve, indicating that the formation and development of shear bands are the precursors of specimen failure.

## 5. Mesopore Structure Changes of Sandstone during Freezing Process

**5.1. NMR Porosity Variation of Saturated Fine Sandstone.** The freezing porosity data of saturated fine sandstone at  $20^{\circ}\text{C}$ ,  $-2^{\circ}\text{C}$ ,  $-5^{\circ}\text{C}$ ,  $-8^{\circ}\text{C}$ ,  $-11^{\circ}\text{C}$ , and  $-15^{\circ}\text{C}$  are shown in Table 2.

It can be seen from Figure 8 that temperature has a great influence on the porosity of fine sandstone at negative temperatures, and the porosity decreases exponentially when the temperature decreases. According to Table 2, from  $20^{\circ}\text{C}$  to  $-15^{\circ}\text{C}$ , the freezing porosity decreases from 9.14% to 1.1%.

When the temperature decreases from  $20^{\circ}\text{C}$  to  $-8^{\circ}\text{C}$ , the porosity decreases sharply and tends to be stable after  $-8^{\circ}\text{C}$ .

**5.2. Pore Throat Distribution.** The micro pore throat structure is the most important factor affecting the macroscopic freeze-thaw physical properties of rock, and the pore size distribution plays an important role in the freezing progress of fine sandstone. The percentage of each pore throat distribution group in the total volume of rock under different temperature conditions of saturated sandstone samples has been shown in Table 3.

It can be seen from Table 3 that the pore throat distribution is different at different temperatures. With the decrease of temperature, the large and medium pore size ( $>10\ \mu\text{m}$  and  $0.1\text{-}10\ \mu\text{m}$ ) decreases sharply, while the small pores ( $<0.1\ \mu\text{m}$ ) increase. The change trend of pore size slows down after  $-8^{\circ}\text{C}$ . At the early freezing stage of the temperature range of  $0^{\circ}\text{C}$  to  $5^{\circ}\text{C}$ , that is, at the rapid freezing stage, the water involved in freezing is mainly free water in large pores, and ice crystals are formed. When the temperature continues to decrease, the water in medium pores freezes, and the ice crystals continue to increase. When the temperature drops below  $-8^{\circ}\text{C}$ , the unfrozen water in the large and medium pore throats continues to freeze into ice, while the bound water content in the small pore throat is still high because its freezing point is low, and the freezing rate is slow. Therefore, the proportion of unfrozen water in small pores is high at lower temperature. The content of each pore size group does not always increase or decrease but fluctuates slightly. The reason for this phenomenon is related to the pore throat distribution of the fine sandstone at room temperature and the conversion rate of fine sandstone from different large pore size groups to adjacent small pore size groups from room temperature to  $-15^{\circ}\text{C}$ .

**5.3. The Relationship between Frozen Sandstone Strength and Micro Structure.** Figure 9 shows the relationship between uniaxial compressive strength and small pore size content in sandstone during freezing. It can be seen from the figure that the proportion of small pores increases with the decrease of porosity, indicating that with the decrease of temperature, ice crystals grow mainly in large and medium pores, and the proportion of large and medium pores decreases, while the proportion of small pores increases. Due to the increase of ice content, rock cohesion and frost heaving force increase, which results in an increase in rock deformation resistance. All these lead to the improvement of uniaxial compressive strength of frozen fine sandstone.

Figure 10 shows the relationship between porosity and uniaxial compressive strength during the freezing process of sandstone. It can be seen from the figure that the porosity of sandstone decreases with the decrease of temperature, while the measured and simulated values of uniaxial compressive strength increase. With the continuous freezing of unfrozen water, the pores are occupied by ice crystals, filling the cracks and pores inside the sample, and the porosity decreases. At the same time, the bonding effect of cracks inside the fine sandstone is improved, and the strength of saturated sandstone is greatly increased. In addition, with

TABLE 3: Table of change in proportion of pore size groups at different temperatures (%).

| Pore size groups ( $\mu\text{m}$ ) | Temperature ( $^{\circ}\text{C}$ ) |      |      |      |      |      |
|------------------------------------|------------------------------------|------|------|------|------|------|
|                                    | 20                                 | -2   | -5   | -8   | -11  | -15  |
| <0.1                               | 10.3                               | 85.6 | 87.4 | 86.8 | 85.4 | 89.1 |
| 0.1-10                             | 26.5                               | 5.8  | 5.6  | 7.6  | 8.9  | 7.0  |
| >10                                | 63.2                               | 8.6  | 7.1  | 5.7  | 5.8  | 3.9  |

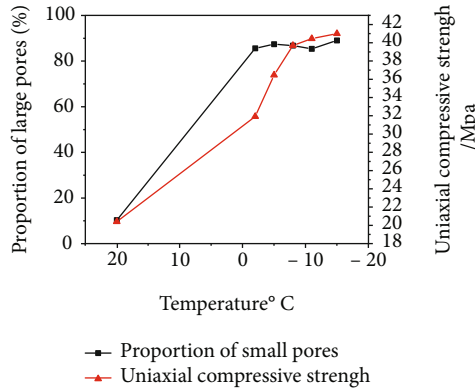


FIGURE 9: Relationship between small pores and uniaxial compressive strength.

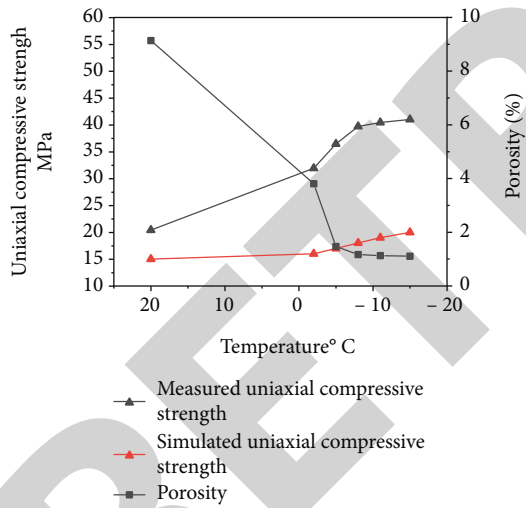


FIGURE 10: Relationship between porosity and uniaxial compressive strength.

the decrease of temperature, the volume of rock particles is compressed, and the arrangement between particles becomes closer, which also makes the strength slightly improved.

When the temperature drops from  $20^{\circ}\text{C}$  to  $-5^{\circ}\text{C}$ , the freezing of the sample is mainly the rapid freezing of water in large pores, which shows a sharp decrease in porosity and also a sharp increase in uniaxial compressive strength. However, at low temperatures, there is still water in pores, and in the range of  $-5^{\circ}\text{C}$  to  $-11^{\circ}\text{C}$ , the unfrozen water in the surrounding micro pores continues to freeze and migrates to the ice crystals in the macro cracks due to the chemical potential. With the temperature decreases continu-

ously, ice in the pores continues to increase, and the measured porosity continues to decrease. Macroscopically, the uniaxial compressive strength continues to increase but the increase rate decreases, because with the continuous decrease of temperature, the amount of unfrozen water in pores is getting less. The content of pore ice in the sample still increases, but the increase is small. At the same time, the changes of porosity and uniaxial compressive strength tend to be stable. Previous studies show that the freezing strength of sandstone has a nonlinear relationship with temperature [26, 27], and the research results of this paper are consistent with them.

## 6. Conclusions

Based on the uniaxial test of frozen sandstone, the mechanical properties of fine sandstone in the freezing process are simulated by using the DEM where the bonding occurs within a limited range of contact particles. Meanwhile, the NMR technique was used to explore the pore distribution inside the frozen fine sandstone. Combined with the DEM results, the microscopic mechanism of the macroscopic mechanical change of fine sandstone was revealed. The main results are as follows:

- (1) The discrete element simulation results are in good agreement with the laboratory test results, which can be used to simulate the mechanical behavior of frozen fine sandstone. The DEM simulation results show that the strength of frozen sandstone increases with the decrease of temperature. With the decrease of temperature, the failure type of fine sandstone changes from plasticity to brittleness. When the temperature is lower than  $-5^{\circ}\text{C}$ , brittle failure happens. With the decrease of temperature, strain softening occurs in frozen sandstone
- (2) DEM simulation shows that with the increase of strain, the micro cracks gradually increase and develop into shear bands. At the same time, the uneven distribution of particle displacement is obvious, and the volume of the sample increases continuously. Finally, a stable shear band from the top left to the bottom right is formed. The corresponding macroscopic deformation occurs after reaching the peak. It shows that the formation and development of shear band is the precursor of failure
- (3) The freezing strength of sandstone has a nonlinear relationship with temperature, and the change of porosity and pore throat distribution can explain the reason. With the decrease of temperature, the large and medium pore size ( $>10 \mu\text{m}$  and  $0.1-10 \mu\text{m}$ ) decreases sharply, and the porosity of sandstone decreases. When the pores and cracks are occupied by ice crystals gradually, the bonding effect of pores and cracks inside the fine sandstone is improved. The cohesion of fine sandstone and frost heaving force increase, which result in an increase in deformation resistance. This is the cause of the

improvement of uniaxial compressive strength of frozen fine sandstone

## Data Availability

The data used to support the findings of this study are available from the corresponding author upon request.

## Conflicts of Interest

The authors declare that they have no conflicts of interest.

## Acknowledgments

This work is supported by the Natural Science Foundation of Anhui Province (Grant Nos. 2008085ME165, 2108085ME185) and the Education Department of Anhui Province (KJ2020A0463).

## References

- [1] Z. S. Yao, H. Cheng, and C. X. Rong, "Shaft structural design and optimization of deep freezing bedrock shaft in west area," *Journal of China Coal Society*, vol. 35, no. 5, pp. 760–764, 2010.
- [2] B. Wang, "Discussion on problems of mine construction in western Chin," *Mine Construction Technology*, vol. 35, no. 1, pp. 49–52, 2014.
- [3] G. S. Yang, J. M. Xi, H. J. Li, and L. Cheng, "Experimental study of rock mechanical properties under triaxial compressive and frozen conditions," *Chinese Journal of Rock Mechanics and Engineering*, vol. 29, no. 3, pp. 459–464, 2010.
- [4] Q. M. Wang, H. Wang, J. Yang, X. Y. Zhang, and X. L. Dong, "Hydrogeochemical characteristics of main water filled aquifers and source indicators of mine water in typical Jurassic mine area of western China," *Journal of Engineering Geology*, vol. 29, no. 4, pp. 1084–1093, 2021.
- [5] M. Y. Ma, Y. S. Huang, G. Y. Cao, J. Lin, and S. Xu, "Study on mechanical behavior of Jurassic frozen sandstone in western China based on NMR porosity," *Journal of Chemistry*, vol. 2020, 2020.
- [6] P. A. Cundall, *The measurement and analysis of acceleration in rock slopes*, Imperial College of Science and Technology, London, England, 1971.
- [7] P. A. Cundall and O. D. L. Strack, "A discrete numerical model for granular assemblies," *Geotechnique*, vol. 29, no. 1, pp. 47–65, 1979.
- [8] M. J. Jiang, "New paradigm for modern soil mechanics: geo-mechanics from micro to macro," *Chinese Journal of Geotechnical Engineering*, vol. 41, no. 2, pp. 195–254, 2019.
- [9] F. X. Zhou and Y. M. Lai, "Simulation of mechanical behavior for frozen sand clay by discrete element method," *Rock and Soil Mechanics*, vol. 31, no. 12, pp. 4016–4020, 2010.
- [10] N. Yin, S. Y. Li, W. S. Pei, M. Zhang, and Y. Dong, "Microscopic deformation mechanisms of triaxial test of frozen clay analyzed by discrete element method," *Journal of Glaciology and Geocryology*, vol. 38, no. 1, pp. 178–185, 2016.
- [11] C. Liu, T. C. Le, B. Shi, and Y. Zhu, "Discussion on three major problems of engineering application of the particle discrete element method," *Chinese Journal of Rock Mechanics and Engineering*, vol. 39, no. 6, pp. 1142–1152, 2020.
- [12] B. Zhou, H. B. Wang, W. F. Zhao, J. W. Li, and B. C. Zheng, "Analysis of relationship between particle mesoscopic and macroscopic mechanical parameters of cohesive materials," *Rock and Soil Mechanics*, vol. 33, no. 10, pp. 3171–3178, 2012.
- [13] C. Y. Kwok and M. D. Bolton, "DEM simulations of soil creep due to particle crushing," *Géotechnique*, vol. 63, no. 16, pp. 1365–1376, 2013.
- [14] N. Belheine, J. P. Plassiard, F. V. Donzé, F. Darve, and A. Seridi, "Numerical simulation of drained triaxial test using 3D discrete element modeling," *Computers and Geotechnics*, vol. 36, no. 1–2, pp. 320–331, 2009.
- [15] J. Kozicki, J. Tejchman, and H. B. Mühlhaus, "Discrete simulations of a triaxial compression test for sand by DEM," *International Journal for Numerical and Analytical Methods in Geomechanics*, vol. 38, no. 18, pp. 1923–1952, 2014.
- [16] J. P. De Bono, G. R. McDowell, and D. Wanatowski, "DEM of triaxial tests on crushable cemented sand," *Granular Matter*, vol. 16, no. 4, pp. 563–572, 2014.
- [17] G. H. Hu, T. Xu, C. F. Chen, and X. K. Yang, "A microscopic study of creep and fracturing of brittle rocks based on discrete element method," *Engineering Mechanics*, vol. 35, no. 9, pp. 26–36, 2018.
- [18] J. Zhou, Y. W. Chi, Y. Chi, and J. P. Xu, "Simulation of biaxial test on sand by particle flow code," *Chinese Journal of Geotechnical Engineering*, vol. 22, no. 6, pp. 701–704, 2000.
- [19] M. Yin, S. Y. Li, Y. H. Shi, Z. Z. Sun, and Z. H. Yin, "Discrete element analysis of cemented behavior of frozen loess under different confining pressures," *Journal of Glaciology and Geocryology*, vol. 39, no. 4, pp. 858–867, 2017.
- [20] W. Yuan, X. L. Yao, and W. L. Wang, "Study on triaxial mechanical behaviors of frozen sand based on discrete element method," *Journal of Glaciology and Geocryology*, vol. 41, no. 6, pp. 1388–1396, 2019.
- [21] T. Wang, Q. Sun, H. Jia, J. Ren, and T. Luo, "Linking the mechanical properties of frozen sandstone to phase composition of pore water measured by LF-NMR at subzero temperatures," *Bulletin of Engineering Geology and the Environment*, vol. 80, no. 6, pp. 4501–4513, 2021.
- [22] H. L. Jia, F. Zi, G. S. Yang et al., "Influence of pore water (ice) content on the strength and deformability of frozen argillaceous siltstone," *Rock Mechanics and Rock Engineering*, vol. 53, no. 2, pp. 967–974, 2020.
- [23] J. F. Lu, C. W. Zhang, and P. Jian, "Meso-structure parameters of discrete element method of sand pebble surrounding rock particles in different dense degrees," in *Proceedings of the 7th International Conference on Discrete Element Methods*, X. Li, Y. Feng, and G. Mustoe, Eds., Springer, Singapore, 2016.
- [24] T. V. Tieng, N. T. T. Hang, and N. X. Khanh, "Compressive behavior of concrete: experimental study and numerical simulation using discrete element method," in *Computational Intelligence Methods for Green Technology and Sustainable Development. GTSD 2020. Advances in Intelligent Systems and Computing*, Y. P. Huang, W. J. Wang, H. A. Quoc, L. H. Giang, and N. L. Hung, Eds., Springer, Cham, 2021.
- [25] H. R. Xiong, K. L. Yuan, M. J. Wen, A. N. Yu, and J. M. Xu, "Influence of pore structure on the moisture transport property of external thermal insulation composite system as studied by NMR," *Construction and Building Materials*, vol. 228, no. 20, pp. 1–9, 2019.

- [26] H. Liu, G. S. Yang, H. L. Jiang et al., "Experimental study on meso-structure of rock in the process of crack (pore) water freezing," *Chinese Journal of Rock Mechanics and Engineering*, vol. 35, no. 2, pp. 2516–2524, 2016.
- [27] H. M. Zhang, H. J. Xia, G. S. Yang, and M. Zhang, "Experimental research of influences of freeze-thaw cycles and confining pressure on physical-mechanical characteristics of rocks," *Journal of China Coal Society*, vol. 43, no. 2, pp. 441–448, 2018.

RETRACTED